Energy efficient nitrogen reduction to ammonia at low overpotential in aqueous electrolyte under ambient conditions

Dabin Wang[a], Luis Miguel Azofra[b], Moussab Harb[b], Luigi Cavallo[b], Xinyi Zhang[a], Bryan H. R. Suryanto[a],*, Douglas R. MacFarlane[a],*

Abstract: The electrochemical nitrogen reduction reaction (NRR) at ambient conditions is a promising alternative to the traditional energy-intensive Haber-Bosch process to produce ammonia. The challenge is to achieve a sufficient energy efficiency, yield rate and selectivity to make the process practical. Herein, we demonstrate that Ruthenium nanoparticles (Ru NPs) enable NRR in 0.01 M HCl aqueous solution at very high energy efficiency, *i.e.*, very low overpotentials. Remarkably, the NRR occurs at potential close to or even above H^+/H_2 reversible potential, significantly enhancing the NRR selectivity versus the production of H_2. NH_3 yield rates as high as ~5.5 mg h^{-1} m^{-2} at 20°C and 21.4 mg h^{-1} m^{-2} at 60°C were achieved at E = -100 mV versus the relative hydrogen electrode (RHE) while a highest Faradaic efficiency of ~5.4% is achievable at E = +10 mV *vs.* RHE. This work demonstrates the potential use of Ru NPs as an efficient catalyst for NRR at ambient conditions. This ability to catalyse NRR at potentials near or above RHE is imperative in improving the NRR selectivity towards a practical process as well as rendering the H_2 viable as by-product. DFT calculations of the mechanism suggest that the efficient NRR process occurring on these predominantly Ru (001) surfaces is catalysed by a d*issociative* mechanism.

Introduction

Ammonia is essential to the agricultural sector as a source of fertiliser,[1] and it is also gaining attention as a promising energy storage medium with high energy density due to the high hydrogen content (17.6 wt.%).[2] As one of the most commonly produced chemical in the world, its handling and transportation are well-developed technologies. However, it is mostly synthesised at industrial scale by the Haber-Bosch process, which is extremely energy and capital intensive.

Electrocatalytic ammonia synthesis at room temperature and atmospheric pressure from N_2 and water has been studied with the goal to achieve more energy-efficient ammonia production. However, with a high dissociation energy of 911 kJ mol^{-1} for the triply bonded dinitrogen molecule, its cleavage is extremely challenging at ambient temperatures and pressures. In addition, the competing H_2 evolution reaction is favoured over NH_3 formation in aqueous electrolytes.[3] To counteract this, an ideal catalyst therefore should have N_2 adsorption on the catalyst surface favoured over hydrogen adsorption.[4] Therefore, the requirements of an effective catalyst are extremely demanding for ammonia synthesis with high activity and selectivity.

Over the last three decades, a number of studies have been published reporting the electrochemical reduction of nitrogen to ammonia. Among these, the most studied is the solid-state electrolyte ammonia synthesis operating at relatively high temperatures.[5] There are comparatively fewer studies on ammonia electrocatalytic synthesis at temperatures below 100°C and even fewer papers on the more challenging synthesis from N_2 and H_2O; that is, without using H_2 as a proton source, the protons instead being generated in situ by water electrolysis. The ability to carry out efficient NRR under ambient conditions with a readily available proton source is critical in a large-scale process that enables the use of NH_3 as medium for the storage of renewable energy. The standard redox potential for the process $N_2 + 8H^+ + 6e^- = 2NH_4^+$ in acid conditions is E = 0.275 – 0.0788pH[6] on the normal hydrogen scale. This indicates that in acid solution the reaction should be feasible at potentials above the H^+/H_2O potential, but this is rarely observed.

In pioneering work by Furuya *et al.* in 1989,[7] the room temperature synthesis of NH_3 from N_2 and H_2 at atmospheric pressure was first realised, however, the lifetime of their catalyst was limited. Following this, in 2000, Kordali and co-workers were the first group to report the room-temperature electrochemical NH_3 synthesis from H_2O and N_2.[8] A maximum rate of 2 mg h^{-1} m^{-2} at 20°C with a low Faradaic efficiency (FE) of only 0.28% was reported with a solid polymer electrolyte cell and electrochemically deposited Ru on carbon felt as catalyst. More recently, Lan *et al.*[9] achieved a significantly higher rate of ~700 mg h^{-1} m^{-2} with FE < 0.1% using Pt as both the cathode when water and air instead of hydrogen and nitrogen were introduced as reactants. However, the use of NH_4^+ pre-treated membrane in that work may explain the unusually high yield rate.

To further boost the reaction rate and efficiency, better catalysts may, ultimately, be the solution for large-scale room temperature ammonia synthesis. Very recently, Chen and co-workers[10] used Fe supported on carbon nanotubes (CNTs) as the catalyst in a flow electrochemical cell operating in the gas phase and a rate of ammonia formation of 2.2 mg h^{-1} m^{-2} was obtained at room temperature and pressure. By using tetrahexahedral gold nanorods (THH Au NRs) as an electrocatalyst, Bao *et al.*[11] achieved a high production yield (NH_3: 16 mg h^{-1} m^{-2} and $N_2H_4 \cdot H_2O$: 1.0 mg h^{-1} m^{-2}) at -0.2 V *vs.* RHE with a FE of ~4% at room temperature and atmospheric pressure. They also investigated Au sub-nanoclusters (≈0.5 nm) embedded on TiO_2 as electrocatalyst,[12] and a rate of 0.021 mg h^{-1} mg^{-1}_{cat} was achieved with a FE of 8.1% at -0.2 V *vs.* RHE.

[a] D. Wang, Dr. X. Zhang, Dr. B. H. R. Suryanto and Prof. D. R. MacFarlane
Australian Centre for Electromaterials Science, School of Chemistry, Monash University, Clayton, VIC 3800 (Australia)
E-mail: douglas.macfarlane@monash.edu; bryan.suryanto@monash.edu
[b] Dr. L. M. Azofra, Dr. M. Harb, Prof. L. Cavallo
KAUST Catalysis Center (KCC), King Abdullah University of Science and Technology (KAUST), Thuwal 23955-6900 (Saudi Arabia)

Industrially, Ru has been widely studied as an alternative to the conventional Fe catalyst for ammonia production, it was demonstrated that Ru-based catalyst are more efficient at lower temperatures.[13] However, the use of Ru for aqueous electrochemical NRR under ambient conditions remains largely unexplored. In this work, the use of Ru NPs as electrocatalysts for NRR in acidic electrolyte was explored. Yield rates of ~5.5 mg h^{-1} m^{-2} at -0.1 V vs RHE and FE of ~5.4% at +0.01 V vs RHE at 25 °C and 21.4 mg h^{-1} m^{-2} at 60°C were thereby achieved. Importantly, these results are achieved at potentials close to RHE, implying higher energy efficiency for the process and making the production of the H_2 by-product viable in energy cost terms. The latter point is a key feature of this report that is frequently overlooked in the literature to date. Hydrogen is the main by-product of all literature reports and it is often implicitly assumed that this has sufficient value as a byproduct to make its production viable. However, this assumption is not necessarily valid because the hydrogen is often produced at overpotentials higher than would be usual for water electrolysis and therefore at higher energy cost. In the work reported here the process is optimized to take place near hydrogen potential and therefore the hydrogen can be considered as an economically viable byproduct that can ultimately be separated from the gas stream by condensation of the NH_3 at lowered temperatures. The results may open up important new directions for the development of practical electrocatalytic ammonia synthesis from nitrogen and water at ambient temperatures and pressures based on Ruthenium.

Results and Discussion

It is known that the interfacial contact between catalyst and carbon based substrate,[14] as well as the use of polymer binders such as Nafion play significant roles in electrocatalysis. Growing nanoparticle directly on the substrate will provide better contacts that would bring about enhanced physical stability and faster electron transfer from active sites to substrate. Hence, Ru NPs were directly grown on the carbon fibre paper (CFP) substrate using an oleate assisted thermal decomposition / reduction method.[15] The Ru^{3+} is reduced in situ while oleate is decomposed at high temperature forming a conductive carbon matrix that also helps to improve the binding strength.[16] By using this in situ synthesis method, the CFP decorated with Ru NPs can be readily used directly as the working electrode for NRR without using any binder.

Figure 1 shows the TEM images of the as-prepared Ru NPs, it is shown that Ru NPs have been uniformly grown exhibiting an average particle size of 2~5 nm. Noticeably, from the high-resolution image in Figure 1b, most of the NPs have a lattice spacing of 2.14 Å, which corresponds to the (002) facet of the hexagonally close packed (*hcp*) Ru (ICDD-JCPDS PDF#06-0663). The diffraction rings in the SAED pattern shown in Figure 1b confirm that all the Ru^{3+} precursors have been fully reduced to form Ru NPs. The XRD pattern (Figure 1c) confirms that the Ru NPs were mainly composed of (002) facets along with part of (102) facets of the hcp Ru which located at 42.2° and 58.3°, respectively. [17]

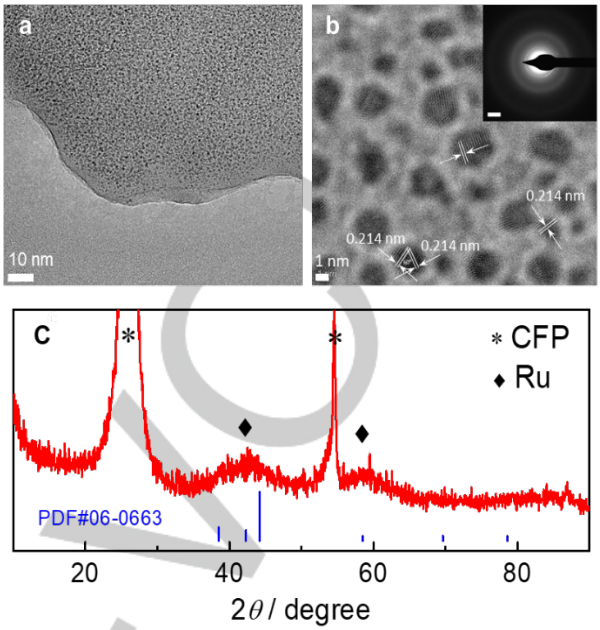

Figure 1. Morphology and structure characterisations of Ru NPs from an oleate-mediated method. (a) TEM and (b) HRTEM image of Ru NPs on CFP. Inserted is the selected area electron diffraction pattern of Ru NPs on CFP (scale bar: 2 1/nm). (c) XRD pattern of Ru NPs on CFP.

The electrocatalytic NRR with Ru NPs was carried out in a three-electrode system with 10 mM hydrochloric acid (HCl) as electrolyte, Pt wire as the counter electrode carrying out water oxidation, which was separated from the working electrode with a glass frit, and Ag/AgCl as the reference electrode. The 10 mM HCl electrolyte we used in all the experiments were unbuffered, therefore it is likely that small local pH changes (<0.5 pH units) will occur in the electrolyte over the course of the electrolysis. The loading of the Ru NPs was determined to be ~1.7 mg cm^{-2} by TGA analysis (Figure S3).

Ultrahigh purity N_2 gas (99.999%) was continuously purged into the electrolyte throughout the experiment. Cyclic voltammetry was first carried out (Figure S4) and not surprisingly, no obvious NRR process could be observed due to the low concentration of N_2 in aqueous solution. To find the optimum potential for NRR, chrono-amperometry (CA) experiments were carried out at a series of different potentials ranging from +50 mV to -600 mV versus RHE. Figure 2a plots the yield rate as a function of the potential. It shows that the yield rate increases with increasing potential towards more negative values and peaks at -100 mV with a rate of ~5.5 mg h^{-1} m^{-2}. Further increase of potential towards more negative values results in lower yield rate as the HER becomes increasingly favoured. The highest FE of ~5.4% was obtained at 10 mV as indicated in Figure 2b. Furthermore, hydrazine (N_2H_4) as a possible intermediate was also detected by the colorimetric method and no N_2H_4 was detected in any experiments (Figure S5), indicating good selectivity towards NRR of the Ru NPs.

It is important to recall that RHE potential, by definition, represents the equilibrium potential at where the net H^+/H_2 current is zero under standard conditions ($P(H_2)$ = 1 bar). In the present case, the hydrogen pressure is much lower than 1 bar in the

electrochemical system; we estimate $p(H_2)$ = 1 x 10^{-5} bar in the +10mV experiment in Figure 2, based on the amount of H_2 produced and the volume of N_2 gas swept through the cell during that experiment. This shifts the equilibrium potential $E(H^+/H_2)$ to +0.15 V vs RHE. Therefore, net hydrogen evolution reaction is still possible at potentials above RHE, such that in that region HER can still contribute to the overall process.

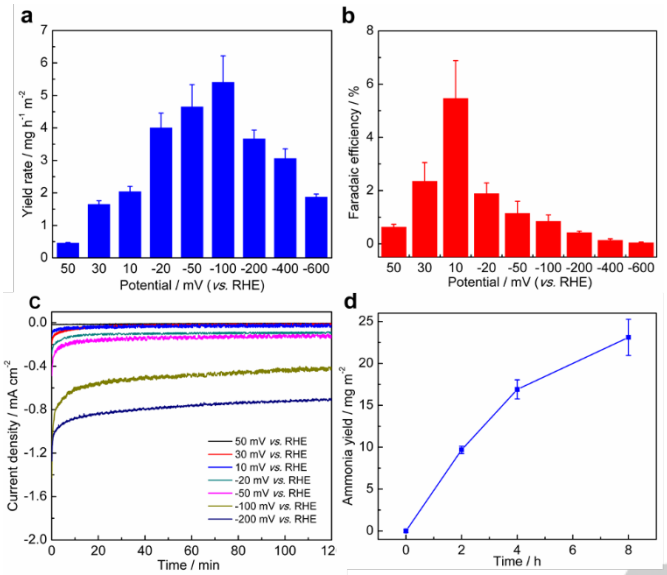

Figure 2. Electrocatalytic NRR performance of Ru NPs. (a) Yield rate at different potentials. (b) Faradaic efficiency at different potentials. (c) Current profiles at different potentials. (d) Ammonia yield as a function of reaction time. (Data = mean and standard deviation of *n* = 3 measurements)

The chronoamperometry in Figure 2c show that the current is stable at various potentials, the decrease of current at higher overpotentials is due to the observable adherence of the as-formed H2 bubbles to the electrode surface resulting in the blockage of the catalytically active sites. Figure 2d shows that Ru NPs can continuously produce ammonia under ambient conditions in aqueous electrolyte. Ammonia was produced at a relatively stable rates in the first 4 hours of experiment as indicated in Figure 2d. However, the NH_3 yield rate was found to decrease slightly at the longer period electrolysis of 8 hours. This decrease could be associated with both (i) a build-up of ammonia in the solution and on the surface of the catalyst thus leading to a decreased yield rate for kinetic reasons and (ii) because of a shift of the local pH at the electrode towards more basic values, shifting the equilibrium N_2/NH_4^+ redox potential more negative and hence lowering the overpotential for the process in this potentiostatic experiment. It is worth noting that the control experiment in which potential bias was not applied and the cell was continuously purged with N_2 for 6 hours, no additional ammonia beyond to that of the background amount was detected (Figure S6).

To further validate the origin of the NH_3, a series of control experiments were conducted to determine the potential contribution of any unexpected NH_3 or N-containing contaminants which might be reduced to NH_3 (*e.g.* NO_x) in the NRR experiments. The UV-Vis curves of the indophenol tests in these control experiments are shown in Figure S7. These control experiments indicate a small adsorption peak, corresponding to a typical background amount of 4~6 nmol NH_3; this is significantly lower than that of our typical NRR experiment yields (up to 60 nmol). The possible NH_3 contributions from the N_2 gas, electrolyte and catalyst are determined and summarized in the Supporting Information and Table S1. It is important to note that neither our electrolyte nor electrode/catalyst materials contain any nitrogen.

Temperature dependence of the ammonia yield rates is shown in Figure 3a, from where we can see the yield rate increases up to 21.4 ± 0.4 mg h^{-1} m^{-2} at 60°C. This further confirms that the NRR in aqueous solution is kinetically limited, and therefore increasing the reaction temperature greatly improves the NRR kinetics, resulting in much enhanced yield rate. However, as temperature is further increased, the solubility of N_2 in water decreases,[18] leading to the decreased yield rate of ~17.8 mg h^{-1} m^{-2} at 80°C.

Additionally, repetitive experiments with the same electrode were carried out to confirm the nitrogen reduction stability of the Ru NPs. As indicated in Figure 3b, the catalyst demonstrated a very stable ammonia yield even after being used for more than ten hours, which confirms that the Ru NPs can effectively produce ammonia over a long period of time. The TEM and XRD characterizations (Figure S8) for the used electrode didn't show any NPs sintering or phase change after the stability test, indicating the catalyst is highly stable. Table S2 summarises the results of NRR under similar conditions in aqueous solution. As

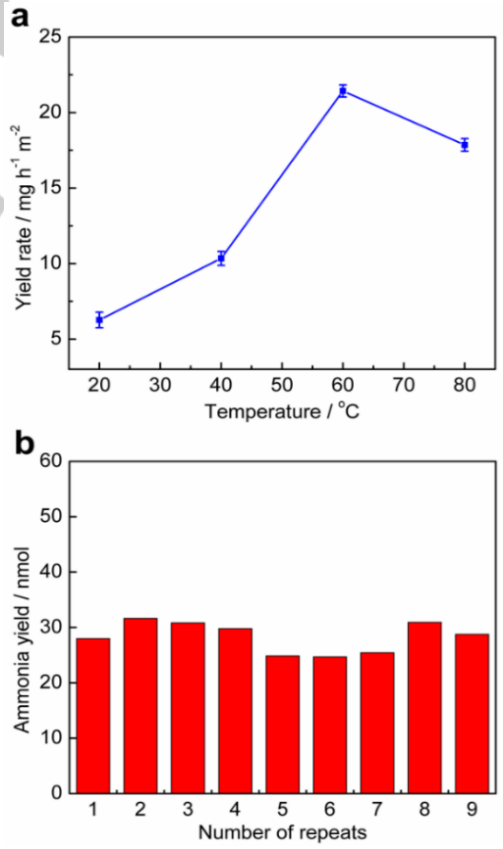

Figure 3. Electrocatalytic NRR performance of Ru NPs. (a) Yield rate at different temperatures at -100 mV for 2 hrs. (b) Ammonia yield of several independent repeats with the same electrode at -100 mV for 2 hrs. (Data = mean and standard deviation of n = 3 measurements)

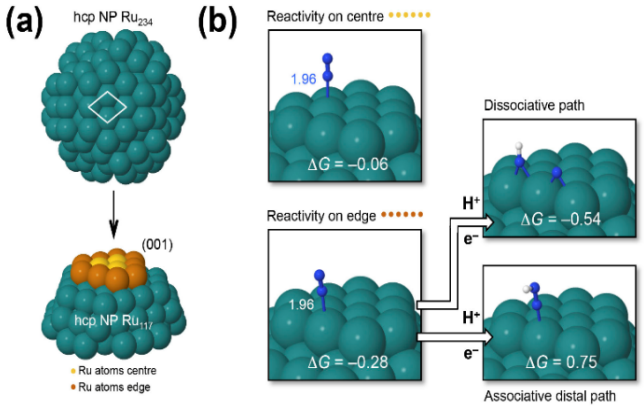

Figure 4. DFT calculation models for Ru NP. (a) hcp Ru_{234} NP and simplified hcp Ru_{117} NP models used in the modelling of NRR. For (001) surface, which is equivalent to (002), two different catalytic sites can be distinguished: centre (yellow) and edge (orange). (b) Structures and Gibbs free energies, in eV, for end-on N_2 adsorption and first hydrogenation steps for the distal *associative* ($*N_2 + H^+/e^- \rightarrow *N_2H$) pathway compared with the *dissociative* ($*N_2 + H^+/e^- \rightarrow *N + *NH$) pathway, with selected distances shown in Å.

can be seen from this data, we have achieved substantial yields of ammonia at potentials as positive as +10 mV vs RHE.

DFT calculations were carried out to better elucidate the reaction mechanisms for NRR catalysed by hcp Ru NPs. As shown in Figure 4a, a *hcp* Ru_{234} NP (234 Ru atoms in the model) was prepared, optimised and later modified towards a simplified model of hcp Ru_{117} NP to analyse the different states during NRR. (See Figure S10 and Supporting Information for full catalyst preparation details). Focusing on the reactivity of the (001) flat surface, which is equivalent to (002), two different types of Ru atoms can be distinguished: those in the centre (highlighted in yellow colour at Figure 4a) and those in the edge (orange). These types of atoms exhibit different catalytic behaviours since they present different atomic environments in the NP. As a result, N_2 adsorption, which is considered the primary stage before starting the electrocatalytic conversion process, shows a Gibbs free binding energy of -0.06 eV when interacting with a Ru atom located at the centre, while this is considerably more spontaneous when happening at the edge, ΔG = -0.28 eV. According to these results, it can be concluded that N_2 adsorption is predominant on the catalytic edge sites of hcp Ru (001) NP. Adsorbed N_2 ($*N_2$) on edge-sites leads to the activation of the N≡N triple bond since it is elongated by 0.02 Å with respect the isolated N_2 molecule in the gas phase. These features of the Ru NPs are likely to be key to the practical NRR performance observed in this work. The elucidation of the NRR mechanism catalysed by *hcp* Ru NP through the edge sides of the (001) surface contemplates two different scenarios. On the one hand, the so-called distal *associative* pathway involves successive hydrogenations of the adsorbed N_2 species without passing from the early N≡N triple bond breakage.[19] Figure 4b contrasts two possible mechanisms for the initial reduction steps: *associative* versus *dissociative*. Figure 4b *associative* indicates that the reduction of $*N_2$ into the $*N_2H$ intermediate species by transfer of the first H^+/e^- pair shows

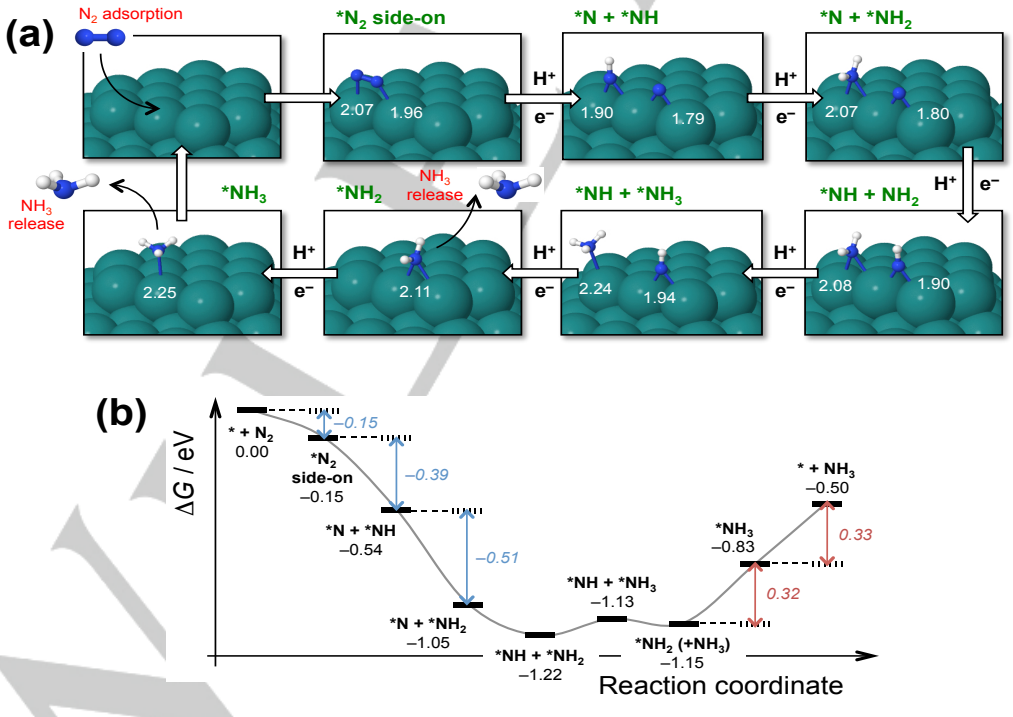

Figure 5. Calculated reaction pathway (*dissociative* mechanism) for NRR on Ru NP. (a) Structures corresponding to the minimum energy pathway (MEP) for catalysed NRR by (001) surface of hcp Ru NP on the edge site. Selected N-Ru distances are indicated in Å. (b) Gibbs free energy diagram for the MEP, in eV, at mild conditions, when there is no applied bias (U = 0 V) and pH = 0. For selected cases, relative free energy changes, $\Delta\Delta G$, are indicated in red (endergonic) and blue (exergonic) colours. Note: '*' denotes adsorbed species on Ru NP.

a Gibbs free reaction energy of 1.03 eV relative to N_2 adsorption, representing the limiting step of this whole associative reaction. (See full path at Figure S11). In this sense, this value highlights the catalytic power of the presented Ru material since it supposes a decrease by around 2 eV with respect to the first hydrogenation in the gas phase (N_2 to N_2H) which has an experimental reduction potential of -3.2 V vs. NHE.[20] Notwithstanding and despite this decrease, this DFT energy prediction contrasts with the very low overpotential that has been experimentally measured for NRR on *hcp* Ru NP.

On the other hand, during the full exploration of the potential energy surface (PES), we noticed a plausible minimum in which the $*N_2H$ species is interacting with two atoms of Ru *via* two N···Ru interactions, leading to the breakage of the dinitrogen bond. This *dissociative* mechanism produces surface nitridation by generation of the [Ru]≡N and [Ru]=NH motifs: $*N_2 + H^+/e^- \rightarrow *N + *NH$. This, which is characterised to be a spontaneous process 0.39 eV downhill with respect to side-on N_2 adsorption, is in the line with what has been recently described by Kitano *et al*. using a Ru-loaded $12CaO{\cdot}7Al_2O_3$ electrode.[21] In this sense, side-on adsorption of N_2 on two Ru atoms, lying at -0.15 eV, is only 0.13 eV above the already described end-on adsorption geometry, and can trigger the transfer of this first H^+/e^- pair (see Figure 5). This indicates the existence of an alternative reaction mechanism consisting of an electrochemically promoted *dissociative* pathway that may be specific to Ruthenium.

This dissociative mechanism follows-up with the second H^+/e^- pair transfer, which is produced on the already hydrogenated N species of *NH. This leads to the surface amination by formation of the [Ru]-NH_2 motif, 0.51 eV downhill with respect to the previous step (see Figure 5). In this regard, the examination of the minimum energy pathway (MEP) reveals that $*N + *NH_2$ intermediate is 0.30 eV more stable than the isoatomic *NH + *NH species. This cascade of spontaneous reactions finishes with the third H^+/e^- pair transfer, that occurs on the un-hydrogenated *N atom to reach $*NH + *NH_2$. This exhibits a Gibbs free energy change of -0.17 eV relative to $*N + *NH_2$.

At this point, the fourth H^+/e^- pair transfer produces the first NH_3 molecule by application of 0.09 eV, and the further second amination by [Ru]-NH_2 formation in the fifth H^+/e^- pair transfer ($\Delta\Delta G$ = -0.02 eV) entails the release of this already formed NH_3 molecule. The mechanism finalises with the last and sixth H^+/e^- pair transfer that generates the second NH_3 molecule, 0.32 eV uphill, and its release, with an energy input of 0.33 eV. This last reduction step, *i.e*., $*NH_2 + H^+/e^- \rightarrow *NH_3$, represents the rate-limiting step of the dissociative mechanism. The good agreement of this energy prediction with the experimental results supports our hypothesis about the existence of an electrochemically promoted dissociative mechanism that is characteristic of Ru as catalyst for NRR at low overpotentials under ambient conditions.

Conclusions

In summary, we have demonstrated that Ru NPs can be an efficient electrocatalyst for the NRR in aqueous media under ambient conditions. The Ru NPs exhibited a highest yield rate of ~5.5 mg h^{-1} m^{-2} at -100 mV vs RHE at room temperature, and the highest FE of ~5.4% at +10 mV vs RHE with a yield rate of ~2 mg h^{-1} m^{-2} was achievable, which is much more efficient than the previously reported electrochemically deposited Ru catalyst with a FE of 0.28%.[8] The low overpotential is related to the instantaneous adsorption and dissociation of N_2 on the edge of Ru NPs, as evidenced by the DFT calculations demonstrating that *hcp* Ru NPs catalyse NRR following an electrochemically promoted *dissociative* pathway. In contrast to the other metal catalysts (e.g., Au, Pd, Pt) where the N_2 adsorption is endothermic and the formation of the first $*N_2H$ species requires huge energy input (>1.2 eV),[11, 22] reactivity on the edge part of Ru (001) surface involves exergonic N_2 adsorption. This is followed by a highly spontaneous process of the hydrogenation of the side-on adsorbed N_2 (-0.9 eV), which automatically leads to the breakage of the dinitrogen bond, demonstrating excellent catalytic ability of Ru NPs for low overpotential NRR under ambient conditions. The results and strategy we report here pave the way to the development of rational catalyst and electrochemical systems which can produce ammonia at a significantly lower energy cost.

Experimental Section

Synthesis of Ru NPs on CFP. An oleate-mediated method was employed to afford better contact between catalyst and substrate. Ruthenium chloride ($RuCl_3{\bullet}xH_2O$), sodium acetate trihydrate ($CH_3CO_2Na{\bullet}3H_2O$), and hexane were purchased from Sigma-Aldrich and used as received. Sodium oleate was used as surfactant and first mixed with $RuCl_3$ in water, then the Ru-oleate was transferred to hexane and loaded onto CFP, after evaporating the solvent for overnight, the Ru-oleate/CFP was put in a tube furnace and calcined at 500°C in Ar for 3 h. The Ru is reduced in situ while oleate is decomposing at high temperature, and the thermal annealing also helps to improve the binding strength. By using this in situ synthesis method, the Ru NPs/CFP composite was obtained and readily used as electrode for NRR without any binder. The loading of the catalyst was determined by TGA.

Electrochemical measurements. The electrochemical reactions were performed in an electrochemical cell, sealed with a Suba seal which allows the system to be isolated from any atmospheric contaminants while purging with N_2 during the experiment, and a water bath was used to maintain constant temperature during the reaction. The cell was equipped with a porous frit to separate the counter electrode from the working electrode, ensuring the products are not re-oxidised on the counter electrode. All electrochemical tests were carried out with a VMP3 multi-channel potentiostat (Bio-Logic Science Instrument) using a three-electrode configuration with platinum wire as counter electrode and Ag/AgCl electrode (saturated KCl electrolyte) as reference electrode. All potentials measured against Ag/AgCl electrode were converted to the RHE reference scale in the report based on the equation: E (vs RHE) =E (vs Ag/AgCl) + 0.197 + 0.059 × pH; pH 2 was used to covert the potentials to the RHE scale. The electrolyte for N_2 reduction experiments (10mL, 10 mM HCl) was pre-saturated with N_2 by purging with N_2 for 30 min before the measurement. Ultrahigh purity Alphagaz N_2 (99.999% purity) was further purified before use with an Agilent oxygen trap and an acid trap to remove the residual O_2 and possible NO_x in the gas stream before being continuously fed to the reaction chamber. A 1 mM HCl trap was used to collect the evaporated ammonia from the gas stream. We have also tested the ammonia retention in 10 mM HCl by purging the electrolyte containing a given amount of ammonia with N_2 for several hours and the result is shown in Figure S9.

Determination of ammonia and hydrazine. Ammonia product was quantitatively determined by the indophenol method.[23] Briefly, 0.5 mL of electrolyte was sampled after the test, followed by addition of 0.5 mL of 0.5 M NaClO, 50 μL of 1 M NaOH solution (with 5 wt.% salicylic acid and 5 wt.% sodium citrate) and 10 μL of 0.5 wt.% $C_5FeN_6Na_2O$ (sodium nitroferricyanide) in water. The mixture was then incubated in the dark at room temperature for 3 h before the UV-vis test.

Calibration curves (Figure S1) were prepared from the same solutions as electrolytes with addition of various concentration of NH_4Cl, and then followed the same procedures as mentioned above. The sample absorbance at 660 nm was used to quantitatively determine the amount of ammonia based on the calibration standards.

Hydrazine (N_2H_4) detection by the Watt and Chrisp method: The colour reagent was prepared by dissolving 0.6 g of para-(dimethylamino) benzaldehyde in 30 mL absolute ethanol with the addition of 3 mL concentrated HCl (32%). Typically, 0.5 mL of the electrolyte solution was taken out and then mixed with 0.5 mL of the above-mentioned colour reagent. Then the mixture was incubated at room temperature in dark for 15 min before the UV-vis test. The solutions of N_2H_4 with known concentrations in 10 mM HCl were used as calibration standards, and the absorbance at λ = 460 nm was used to plot the calibration curves (Figure S2).

Calculation of Faradaic efficiency. To define the Faradaic efficiency for NRR, the amount of charge used for ammonia production was divided by the total charge passed through the electrodes during the electrolysis. Given that the formation one NH_3 needs three electrons, the Faradaic efficiency can be calculated as follows: Faradaic efficiency = $Q_{NH3}/Q_{total} = \frac{3\times F\times m}{Q_{total}} \times 100\%$, where F is the Faraday constant and m is the amount of ammonia detected in the experiment.

Computational methods. The mechanism for N_2 adsorption and its further electrochemical conversion into NH_3 catalysed by (001) surface of a hexagonal close-packed (hcp) Ru nanoparticle (NP), was studied by means of density functional theory (DFT). The generalised-gradient approximation (GGA) within the revised Perdew-Burke-Ernzerhof (revPBE) exchange-correlation functional[24] and the standard frozen-core projector augmented-wave (PAW) approach[25] were adopted, respectively, for electron-electron and electron-ion interaction descriptions. The configurations of valence electrons taken explicitly into account in our calculations were $4d^7 5s^1$ for Ru, $2s^2 2p^3$ for N and ultrasoft $1s^1$ for H. A plane-wave cut-off energy up to 400 eV was expanded for electron wave-functions.[26] Full structural optimisation calculations were performed when the force components on each species were less than 0.01 eV $Å^{-1}$, the stress was less than 0.01 GPa, the energy change per species less than 1 meV and the displacement less than 10^{-4} Å. In all cases, spin-polarised considerations were taken into account, concluding that there are no magnetisation effects as well as changes in the electronic energies. Over these optimised structures, vibrational frequencies were calculated in order to obtain zero-point energies (ZPE), thermal corrections and entropy contributions. At this step, explicit dispersion correction terms to the energy were also employed through the use of the D3 method with the standard parameters programmed by Grimme and co-workers.[27] All Gibbs free energy values for the N_2 reduction mechanism were referenced to the computational hydrogen electrode (CHE) model using the proton-coupled electron transfer (PCET) approach.[28] All optimisation and vibrational frequency calculations were performed using the Vienna *Ab-Initio* Simulation Package (VASP, version 5.4.1).[29]

Acknowledgements

The authors thank Monash Centre for Electron Microscopy (MCEM) for the provision of access to their instruments. L.M.A., M.H. and L.C. acknowledge King Abdullah University of Science and Technology (KAUST) for support. Gratitude is also due to the KAUST Supercomputing Laboratory using the supercomputer Shaheen II for providing the computational resources. This study was supported by an Australian Research Council (ARC) Discovery Grant (DP170102267). D.R.M. is grateful to the ARC for his Australian Laureate Fellowship.

Keywords: nitrogen reduction reaction• ammonia synthesis • ambient conditions • electrochemical • nitrogen fixation

[1] S. Giddey, S. Badwal, A. Kulkarni, *Int. J. Hydrog. Energy* **2013**, *38*, 14576-14594.

[2] a) W. Avery, *Int. J. Hydrog. Energy* **1988**, *13*, 761-773; b) R. Lan, J. T. Irvine, S. Tao, *Int. J. Hydrog. Energy* **2012**, *37*, 1482-1494; c) C. H. Christensen, T. Johannessen, R. Z. Sørensen, J. K. Nørskov, *Catal. Today* **2006**, *111*, 140-144.

[3] B. H. R. Suryanto, C. S. M. Kang, D. Wang, C. Xiao, F. Zhou, L. M. Azofra, L. Cavallo, X. Zhang, D. R. MacFarlane, *ACS Energy Lett.* **2018**.

[4] E. Skulason, T. Bligaard, S. Gudmundsdottir, F. Studt, J. Rossmeisl, F. Abild-Pedersen, T. Vegge, H. Jonsson, J. K. Norskov, *Phys. Chem. Chem. Phys.* **2012**, *14*, 1235-1245.

[5] a) I. A. Amar, R. Lan, C. T. Petit, S. Tao, *J. Solid State Electrochem.* **2011**, *15*, 1845; b) I. Garagounis, V. Kyriakou, A. Skodra, E. Vasileiou, M. Stoukides, *Frontiers in Energy Research* **2014**, *2*.

[6] M. Pourbaix, *Corrosion Engineers, Houston* **1974**.

[7] N. Furuya, H. Yoshiba, *149.* *J. Electroanal. Chem. Interfac.* **1989**, *263*, 171-174.

[8] V. Kordali, G. Kyriacou, C. Lambrou, *Chem. Commun.* **2000**, 1673-1674.

[9] R. Lan, J. T. Irvine, S. Tao, *Sci. Rep.* **2013**, *3*, 1145.

[10] S. Chen, S. Perathoner, C. Ampelli, C. Mebrahtu, D. Su, G. Centi, *Angew. Chem.* **2017***,* 129, 2743*; Angew. Chem. Int. Ed.* **2017**, *56*, 2699-2703.

[11] D. Bao, Q. Zhang, F. L. Meng, H. X. Zhong, M. M. Shi, Y. Zhang, J. M. Yan, Q. Jiang, X. B. Zhang, *Adv. Mater.* **2017**, *29*, 1604799.

[12] M. M. Shi, D. Bao, B. R. Wulan, Y. H. Li, Y. F. Zhang, J. M. Yan, Q. Jiang, *Adv. Mater.* **2017**.

[13] a) F. Rosowski, A. Hornung, O. Hinrichsen, D. Herein, M. Muhler, G. Ertl, *Applied Catalysis A: General* **1997**, *151*, 443-460; b) G. Rambeau, H. Amariglio, *Applied Catalysis* **1981**, *1*, 291-302; c) H. Bielawa, O. Hinrichsen, A. Birkner, M. Muhler, *Angew. Chem.* **2001** 113: 1093-1096; *Angew. Chem. Int. Ed.* **2001**, *40*, 1061-1063.

[14] B. H. R. Suryanto, S. Chen, J. Duan, C. Zhao, *ACS Appl. Mater. Interfaces* **2016**, *8*, 35513-35522.

[15] J. Park, K. An, Y. Hwang, J.-G. Park, H.-J. Noh, J.-Y. Kim, J.-H. Park, N.-M. Hwang, T. Hyeon, *Nat Mater.* **2004**, *3*, 891.

[16] J. Li, Y. Wang, T. Zhou, H. Zhang, X. Sun, J. Tang, L. Zhang, A. M. Al-Enizi, Z. Yang, G. Zheng, *J. Am. Chem. Soc.* **2015**, *137*, 14305-14312.

[17] M. Zhao, A. O. Elnabawy, M. Vara, L. Xu, Z. D. Hood, X. Yang, K. D. Gilroy, L. Figueroa-Cosme, M. Chi, M. Mavrikakis, *Chem. Mater.* **2017**, *29*, 9227-9237.

[18] H. A. Pray, C. Schweickert, B. Minnich, *Ind. Eng. Chem. Res.* **1952**, *44*, 1146-1151.

[19] J. H. Montoya, C. Tsai, A. Vojvodic, J. K. Norskov, *ChemSusChem* **2015**, *8*, 2180-2186.

[20] C. J. van der Ham, M. T. Koper, D. G. Hetterscheid, *Chem. Soc. Rev.* **2014**, *43*, 5183-5191.

[21] M. Kitano, S. Kanbara, Y. Inoue, N. Kuganathan, P. V. Sushko, T. Yokoyama, M. Hara, H. Hosono, *Nat commun.* **2015**, *6*, 6731.

[22] J. Wang, L. Yu, L. Hu, G. Chen, H. Xin, X. Feng, *Nat Commun.* **2018**, *9*, 1795.

[23] H. Verdouw, C. Van Echteld, E. Dekkers, *Water Res.* **1978**, *12*, 399-402.

[24] J. P. Perdew, K. Burke, M. Ernzerhof, *Phys. Rev. Lett.* **1996**, *77*, 3865.

[25] P. E. Blöchl, *Phys. Rev. B* **1994**, *50*, 17953.

[26] G. Kresse, D. Joubert, *Phys. Rev. B* **1999**, *59*, 1758.

[27] a) S. Grimme, J. Antony, S. Ehrlich, H. Krieg, *J. Chem. Phys.* **2010**, *132*, 154104; b) S. Grimme, S. Ehrlich, L. Goerigk, *J. Comput. Chem.* **2011**, *32*, 1456-1465.

[28] A. A. Peterson, F. Abild-Pedersen, F. Studt, J. Rossmeisl, J. K. Nørskov, *Energy Environ. Sci.* **2010**, *3*, 1311-1315.

[29] a) G. Kresse, J. Hafner, *Phys. Rev. B* **1993**, *47*, 558; b) G. Kresse, J. Hafner, *Phys. Rev. B* **1994**, *49*, 14251-14269; c) G. Kresse, J. Furthmüller, *Phys. Rev. B* **1996**, *54*, 11169-11186; d) G. Kresse, J. Furthmüller, *Comput. Mater. Sci.* **1996**, *6*, 15-50.

FULL PAPER

Electrochemical nitrogen reduction reaction (NRR) on Ruthenium nanoparticles was studied experimentally, together with theoretical density functional theory (DFT) calculation, demonstrating the possibility of using Ru as catalyst for ammonia synthesis under ambient conditions.

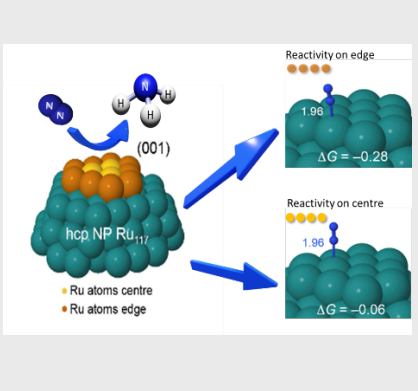

Dabin Wang[a], Luis Miguel Azofra[b], Moussab Harb[b], Luigi Cavallo[b], Xinyi Zhang[a], Bryan H. R. Suryanto[a],*, Douglas R. MacFarlane[a],*

Page No. – Page No.

Energy efficient nitrogen reduction to ammonia at low overpotential in aqueous electrolyte under ambient conditions